A Distinct Advantage to Intraarterial Delivery of ^{89}Zr-Bevacizumab in PET Imaging of Mice With and Without Osmotic Opening of the Blood–Brain Barrier

Wojciech G. Lesniak[1], Chengyan Chu[1,2], Anna Jablonska[1,2], Yong Du[1], Martin G. Pomper[1], Piotr Walczak[1–3], and Miroslaw Janowski[1,2,4]

[1]Russell H. Morgan Department of Radiology and Radiological Science, Johns Hopkins University School of Medicine, Baltimore, Maryland; [2]Institute for Cell Engineering, Johns Hopkins University School of Medicine, Baltimore, Maryland; [3]Department of Neurosurgery, University of Warmia and Mazury, Olsztyn, Poland; and [4]NeuroRepair Department, Mossakowski Medical Research Centre, Polish Academy of Sciences, Warsaw, Poland

See an invited perspective on this article on page 615.

Glioblastoma multiforme (GBM) is the most aggressive and common type of brain cancer. Five-year survival rates are below 12%, even with the most aggressive trimodal therapies. Poor blood–brain barrier (BBB) permeability of therapeutics is a major obstacle to efficacy. Intravenous administration of bevacizumab is the standard treatment for GBM. It has been recently demonstrated that a single intraarterial infusion of bevacizumab provides superior therapeutic outcomes in patients with recurrent GBM. Further GBM treatment benefits can be achieved through opening of the BBB before intraarterial infusion of bevacizumab. However, a rationale for intraarterial delivery and BBB opening when delivering antibodies is lacking. A method facilitating quantification of intraarterial delivery of bevacizumab is needed for more effective and personalized GBM treatment. Here, we demonstrate such a method using PET imaging of radiolabeled bevacizumab. **Methods:** Bevacizumab was conjugated with deferoxamine and subsequently radiolabeled with ^{89}Zr. ^{89}Zr-bevacizumab deferoxamine (^{89}Zr-BVDFO) was prepared with a specific radioactivity of 81.4 ± 7.4 MBq/mg (2.2 ± 0.2 μCi/mg). Brain uptake of ^{89}Zr-BVDFO on carotid artery and tail vein infusion with an intact BBB or with BBB opening with mannitol was initially monitored by dynamic PET, followed by whole-body PET/CT at 1 and 24 h after infusion. Th ex vivo biodistribution of ^{89}Zr-BVDFO was also determined. **Results:** Intraarterial administration of ^{89}Zr-BVDFO resulted in gradual accumulation of radioactivity in the ipsilateral hemisphere, with 9.16 ± 2.13 percentage injected dose/cm^3 at the end of infusion. There was negligible signal observed in the contralateral hemisphere. BBB opening with mannitol before intraarterial infusion of ^{89}Zr-BVDFO resulted in faster and higher uptake in the ipsilateral hemisphere (23.58 ± 4.46 percentage injected dose/cm^3) and negligible uptake in the contralateral hemisphere. In contrast, intravenous infusion of ^{89}Zr-BVDFO and subsequent BBB opening did not lead to uptake of radiotracer in the brain. The ex vivo biodistribution results validated the PET/CT studies. **Conclusion:** Our findings demonstrate that intraarterial delivery of bevacizumab into the brain across an osmotically opened BBB is effective, in contrast to the intravenous route.

Received Aug. 1, 2018; revision accepted Sep. 24, 2018.
For correspondence or reprints contact: Miroslaw Janowski, Johns Hopkins University, 1550 Orleans St., CRB II 4M63, Baltimore, MD 21231.
E-mail: mjanows1@jhmi.edu
Published online Oct. 12, 2018.

Key Words: nuclear medicine; molecular imaging; endovascular; drug delivery; brain

J Nucl Med 2019; 60:617–622
DOI: 10.2967/jnumed.118.218792

Although there has been significant progress in the treatment of various neoplastic diseases, glioblastoma multiforme (GBM) remains incurable (*1*). Treatment of GBM is particularly challenging because it often resides behind the blood–brain barrier (BBB). Poor penetration of therapeutic agents across the BBB is a major obstacle to therapy of brain tumors. An effective route to deliver the rapidly growing portfolio of therapeutic agents for GBM is needed.

Several advanced methods for drug delivery to the brain have been developed, including stereotactic convection-enhanced delivery (*2*), slow-release polymers (*3*), polymeric micelles (*4*), focused ultrasound (*5*), and intraarterial administration (*6*). Among these methods, the intraarterial route has the longest history and seemed an intuitive way to achieve high drug concentrations in the brain while minimizing systemic toxicity (*7,8*). The discovery of reversible osmotic BBB opening was a further improvement (*9*). However, some studies led to white matter necrosis and blindness and revealed a lack of technical means for precise catheter placement, thus diminishing enthusiasm about intraarterial administration (*10*). Progress in the development of new drugs and improved endovascular catheters, along with the persistent lack of effective therapeutic options for brain cancers, has now resulted in renewed interest in intraarterial drug delivery (*11,12*). In an early study, Burkhardt et al. showed that the therapeutic efficacy of a single intraarterial infusion of bevacizumab matched that of repetitive systemic injections and was superior to a single intravenous administration in the U87 xenograft mouse model (*13*). A more recent study by Chakraborty et al. demonstrated that intraarterial BBB opening followed by a high dose of bevacizumab was at least as effective as repetitive systemic injections for the treatment of recurrent glioblastoma while virtually eliminating any adverse systemic effects (*14*).

PET has long been used in clinical studies to determine target engagement of drugs and other therapeutics intended for brain

activity (*15*). Radiolabeling of monoclonal antibodies with the relatively long-lived radionuclide ^{89}Zr has been used to evaluate their targeting properties (*16*). ^{89}Zr-bevacizumab deferoxamine (BVDFO) has been shown clinically to accumulate specifically in breast cancer, renal cell carcinoma, and non–small cell lung cancer, allowing expression of vascular endothelial growth factor (VEGF)–A to be determined as an indication of therapeutic efficacy (*17–19*). However, variably low or no uptake of ^{89}Zr-BVDFO in brain lesions was demonstrated in children with diffuse intrinsic pontine glioma (*20*), in agreement with other studies showing no ^{89}Zr-BVDFO accumulation in intracranial tumors in mice with the same tumor model after systemic delivery (*21*). Here, we used ^{89}Zr-BVDFO and PET to capture the dynamics of bevacizumab after intraarterial delivery to the brain and compared its brain distribution with and without BBB opening. We also compared intraarterial and systemic (intravenous) delivery under the same conditions.

MATERIALS AND METHODS

Materials

All chemicals were purchased from Sigma-Aldrich or Fisher Scientific unless otherwise specified. Bevacizumab (Avastin [Roche]; 4 mL, 25 mg/mL) was obtained from Johns Hopkins Hospital Pharmacy. $^{89}Zr(C_2O_4)_2$ (half-life, 78.4 h) and 1-(4-isothiocyanatophenyl)-3-[6,17-dihydroxy-7,10,18,21-tetraoxo-27-(*N*-acetylhydroxylamino)-6,11,17,22-tetraazaheptaeicosine]thiourea (p-SCN-Bn-deferoxamine, catalog number B-705) were obtained from Washington University and Macrocyclics, respectively. All reagents and solvents were used as received, without further purification.

Study Design

In the first step, we conjugated bevacizumab with deferoxamine chelator and characterized the resulting conjugate by means of its molecular weight and binding to VEGF. After radiolabeling of the conjugate with ^{89}Zr, we evaluated accumulation in the brain using 3 groups of mice ($n = 4$). The first group was treated with intraarterial infusion of ^{89}Zr-BVDFO with an intact BBB (IA/BBBI). The second group was treated with intraarterial infusion of ^{89}Zr-BVDFO immediately after BBB opening with 25% mannitol (BBBO/IA). The third group was treated with intravenous infusion of ^{89}Zr-BVDFO and subsequent BBB opening with mannitol at a 15-min interval (IV/BBBO), which allowed assessment of brain uptake of ^{89}Zr-BVDFO before and after BBB opening in the same animals. Accumulation of radioactivity in the brain during and after infusion of ^{89}Zr-BVDFO reconstituted in 1 mL of saline and delivered at 0.15 mL/min was monitored by dynamic (1 bed position) PET over 0.5 h and subsequent whole-body (2 bed positions) volume-rendered PET/CT. On the next day, PET/CT was repeated, the animals were sacrificed, and the ex vivo biodistribution of ^{89}Zr-BVDFO was determined.

Synthesis of BVDFO

The Avastin brand of bevacizumab is formulated in 240 mg of α,α-trehalose dehydrate, 23.2 mg of sodium phosphate (monobasic, monohydrate), 4.8 mg of sodium phosphate (bibasic, anhydrous), 1.6 mg of polysorbate 20, and water. For conjugation with deferoxamine, 15 mg of the antibody were purified using ultrafiltration with Millipore Amicon Ultra Centrifugal Filters 50K (catalog number VV-29969-76) and saline. After purification, 10 mg of bevacizumab were reconstituted in 2 mL of saline, pH was adjusted to 9 with a small amount of 0.1 M Na_2CO_3, a 5-fold molar equivalent of SCN-Bn-deferoxamine dissolved in dimethyl sulfoxide was added, and conjugation was performed for 30 min at 37°C in a thermomixer at 550 rpm. The resulting BVDFO conjugate was purified as described above and reconstituted in saline at 10 mg/mL, and 0.1-mL aliquots were kept at −20°C until further use. The protein concentration in the purified bevacizumab and the BVDFO conjugate was determined by absorbance at 280 nm, obtained by collecting the ultraviolet–visible spectrum ranging from 200 to 750 nm and the extinction coefficient of 1.52 cm × mL/mg derived from the law of Beer and the 280-nm absorbance of a 2.5 mg/mL solution of bevacizumab in phosphate-buffered saline.

Matrix-Assisted Laser Desorption Ionization Time-of-Flight Spectrometry

To determine the average number of deferoxamine molecules conjugated with bevacizumab, matrix-assisted laser desorption ionization time-of-flight spectra of the unmodified antibody and the BVDFO conjugate were recorded on a Voyager DE-STR spectrophotometer, using 2,5-dihydroxybenzoic acid as a matrix. First, protein samples were desalted using Zeba spin columns (7-kDa molecular weight cutoff, catalog number 89882; Thermo Fisher Scientific), and 10 μL of elutes were mixed with 10 μL of matrix (10 mg/mL). Then, 1 μL of the resulting mixture was placed on the target plate (in triplicate) and evaporated. The matrix was dissolved in 50% MeOH and 0.1% trifluoroacetic acid aqueous solution. The number of shots and laser power were adjusted according to spectrum quality.

Functional Binding Assay of Bevacizumab and BVDFO to VEGF

The ELISA devoted to assessment of bevacizumab concentrations (ImmunoGuide; Eagle Bioscience) was used to assess the binding capacity of unmodified bevacizumab and the BVDFO conjugate. The assay was performed according to the manufacturer's protocol. Briefly, 100, 50, and 25 μg/mL concentrations of bevacizumab and BVDFO, as well as the provided standards, were diluted 1:1,000 and pipetted in 6 repetitions into the wells of the microtiter plate coated with recombinant human VEGF-A. The plate was incubated for 60 min at room temperature and washed 3 times with buffer. Next, horseradish peroxidase–conjugated antihuman IgG monoclonal antibody was added to each well and incubated at room temperature for 30 min. The plate was washed 3 times with the buffer, and ready-to-use 3,3′,5,5′-tetramethylbenzidine substrate solution was added to each well. After 15 min of incubation in the dark, stop solution was added to each well and the color change from blue to yellow was observed. The absorbance at 450 nm was read using a Victor 3 plate reader (Perkin Elmer) within 10 min after addition of the stop solution and was expressed as optical density.

Radiolabeling of BVDFO

BVDFO was radiolabeled with ^{89}Zr using a modification of a reported procedure (*16*). The protein concentration in the obtained ^{89}Zr-BVDFO was determined on the basis of absorbance at 280 nm from an ultraviolet–visible spectrum collected on a Nanodrop 2000 ultraviolet–visible spectrophotometer (Thermo Fisher Scientific) and the area under the peak in a size-exclusion chromatogram recorded using absorbance at 280 nm. Size-exclusion chromatography was performed using a Varian ProStar pump, a Phenomenex Yarra SEC-4000 column, and 0.1 M phosphate buffer (pH 6.4) as a mobile phase at a flow rate of 1 mL/min. Elution was monitored using a Varian ProStar ultraviolet absorbance detector set to 280 nm and a radioactive single-channel flow-through radiation detector (Bioscan model 105S). ^{89}Zr-BVDFO was fabricated with 99.4% radiochemical purity and an 81.4 ± 7.4 MBq/mg (2.2 ± 0.2 μCi/mg) specific activity. For further studies, ^{89}Zr-BVDFO was diluted with sterile saline.

PET/CT Imaging of Intraarterial and Intravenous Delivery of ^{89}Zr-BVDFO With and Without BBB Opening

All animal procedures were performed under protocols approved by the Johns Hopkins Animal Care and Use Committee. Under general

anesthesia with 1%–2% isoflurane, a catheter was placed in the internal carotid artery of male C3HeB/FeJ mice (stock number 000658; Jackson), 6–8 wk old, as we described previously (*22*), and each animal was transferred to the PET/CT scanner. The BBB was opened with a minute-long infusion of 25% mannitol at a speed 0.15 mL/min. Approximately 8.5 MBq (~230 μCi) of ^{89}Zr-BVDFO reconstituted in 1 mL of saline was infused intraarterially or intravenously over 5 min, also at a speed of 0.15 mL/min. Accumulation of ^{89}Zr-BVDFO in the brain was initially monitored with dynamic scans. For intraarterial infusions, 30-s frames at 1 bed position were collected for 30 min; for intravenous infusions, 30-s frames at 1 bed position were collected for 45 min: 15 min before BBB opening and 30 min after BBB opening. Whole-body PET/CT imaging was then performed at around 1 h after infusion, at 2 bed positions and at a rate of 7 min per bed position, on an ARGUS small-animal PET/CT scanner (Sedecal). A CT scan (512 projections) was performed after the dynamic scan for anatomic coregistration. PET/CT imaging was repeated at around 24 h after infusion. PET data were reconstructed using 2-dimensional ordered-subsets expectation maximization and corrected for dead time and radioactive decay. The presented whole-body images were generated using Amira (FEI) and the dynamic scans (brain and heart radioactivity accumulation), and the radioactivity distribution in different brain regions was analyzed with PMOD, version 4.3 (PMOD Technologies LLC).

Ex Vivo Biodistribution of ^{89}Zr-BVDFO

On completion of PET/CT at 24 h after infusion of ^{89}Zr-BVDFO, the mice were sacrificed, and blood, brain (divided into right and left hemispheres), and selected organs were harvested and weighed. The radioactivity in the collected samples was measured on a PerkinElmer 2480 automatic γ-counter. To calculate the percentage injected dose per cubic centimeter of tissue (%ID/g), triplicate radioactive standards (0.01% of the injected dose) were counted along with tissue samples. The biodistribution data shown are mean ± SEM.

Statistical Analysis

PROC MIXED (SAS, version 9.4) was used for statistical analysis, with the lowest-mean-square test for comparisons between groups. The terms *repeated* and *random* were used for repeated measures and to express random effects, respectively.

RESULTS

Radiolabeling

As depicted in Figure 1A, radiolabeling of bevacizumab with ^{89}Zr involved conjugation on an average of 3 molecules of deferoxamine and subsequent chelation of $^{89}Zr^{4+}$. The average number of deferoxamine molecules conjugated with bevacizumab was derived from the increase in molecular weight detected by matrix-assisted laser desorption ionization time-of-flight spectrometry (Fig. 1C). Bevacizumab and the BVDFO conjugate exhibited similar binding to VEGF as confirmed by ELISA (Fig. 1D). Coelution of ^{89}Zr-BVDFO with intact bevacizumab observed in the size-exclusion chromatogram confirmed radiolabeling of BVDFO (Fig. 1E). ^{89}Zr-BVDFO was prepared at 81.4 ± 7.4 MBq/mg and at 99% ± 2% and 73% ± 3% specific activity (radiochemical purity and efficiency, respectively).

PET Imaging

IA/BBBI resulted in a gradual accumulation of radioactivity during infusion in the ipsilateral hemisphere, reaching 9.66 ± 2.04 %ID/cm^3 between the first and sixth minutes after infusion was completed. The signal remained stable thereafter, and between the 20th and 25th minutes it equaled 9.16 ± 2.13 %ID/cm^3 (P = 0.3) (Figs. 2A and 2D). There was negligible signal observed in the contralateral hemisphere. BBBO/IA resulted in faster and significantly higher uptake of radioactivity in the ipsilateral hemisphere, reaching 23.58 ± 4.58 %ID/cm^3 between the first and sixth minutes after infusion was completed and remaining stable thereafter, at 23.58 ± 4.46 %ID/cm^3 (P = 0.99) (Figs. 2B and 2D). Similarly to IA/BBBI, no uptake in the contralateral hemisphere was observed. In contrast, there was no preferential uptake on IV/BBBO in any hemisphere either before or after BBB opening, and only background was detected in the entire brain (before BBB opening, 2.91 %ID/cm^3; afterward, 2.91 %ID/cm^3; P = 0.99) (Figs. 2C and 2D). The expected gradual increase of radioactivity in the heart during infusion was seen in all 3 groups, with subsequent stabilization (Fig. 2E). Figure 3 contains representative PET images overlaid by the mouse brain template available in PMOD 4.3, with an associated bar graph illustrating the difference in uptake in different brain regions 1 h after infusion. Uptake was significantly higher in the BBBO/IA group than in the other 2 groups, being highest in the right striatum (16.92 ± 5.7 %ID/cm^3), right hippocampus

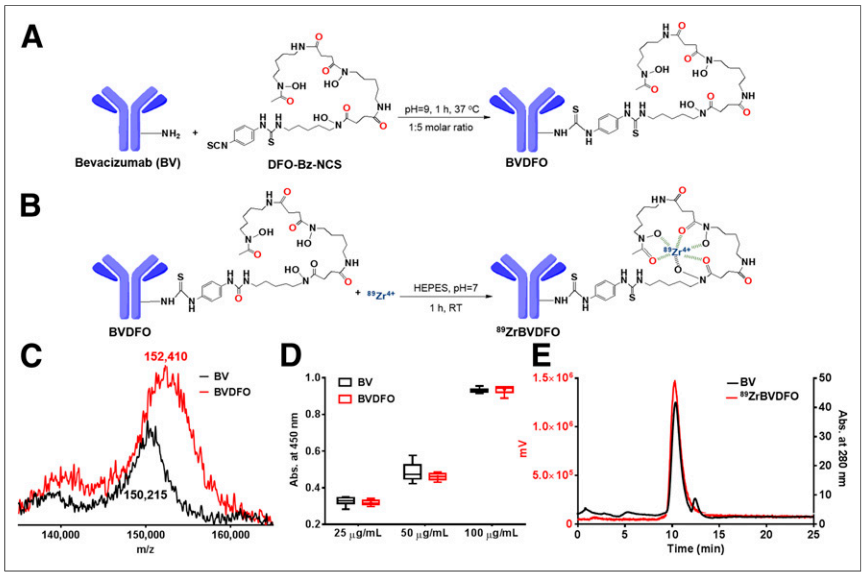

FIGURE 1. Radiolabeling of bevacizumab with ^{89}Zr. (A and B) Reaction schemes demonstrating conjugation of bevacizumab with deferoxamine and its subsequent radiolabeling with ^{89}Zr. (C) Matrix-assisted laser desorption ionization time-of-flight spectra of bevacizumab and BVDFO, showing increase of molecular weight that indicates conjugation on average of 3 molecules of deferoxamine with each antibody. (D) Evaluation of bevacizumab and BVDFO biding to VGEF, showing that conjugation of deferoxamine with antibody did not affect its targeting properties. (E) Size-exclusion chromatograms illustrating coelution of bevacizumab (black line, based on absorbance at 280 nm) and ^{89}Zr-BVDFO (red line, derived using flow-through radiation detector), indicating successful radiolabeling of BVDFO with ^{89}Zr. RT = room temperature; HEPES = 4-(2-hydroxyethyl)-1-piperazineethanesulfonic acid.

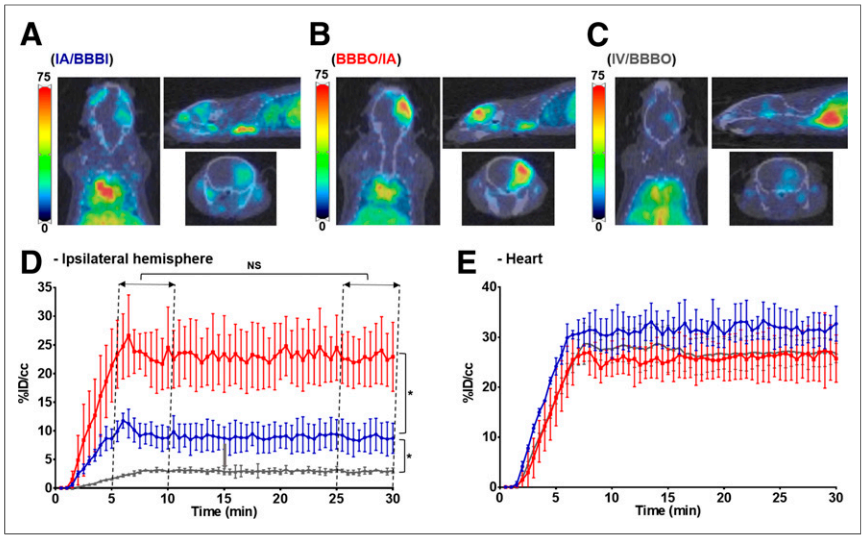

FIGURE 2. Dynamics of ^{89}Zr-BVDFO delivery with and without BBB opening. (A–C) Representative axial, sagittal, and coronal PET/CT images showing brain uptake with IA/BBBI (A), BBBO/IA (B), and IV/BBBO (C). (D) Graph showing faster and higher ipsilateral hemisphere uptake with BBBO/IA (red) than with IA/BBBI (blue) or IV/BBBO (gray). (E) Graph showing increase in heart uptake with IA/BBBI (blue), BBBO/IA (red), and IV/BBBO (gray) (n = 4). No increase in brain uptake was observed with IV/BBBO on 45-min dynamic PET scans. NS = statistically nonsignificant. *Statistically significant difference.

(15.64 ± 3.15 %ID/cm^3), and right amygdala (12.27 ± 2.77 %ID/cm^3). In the IA/BBBI group, uptake was highest in the right hippocampus, reaching only 8.4 ± 1.75 %ID/cm^3. In contrast, the IV/BBBO group showed only negligible uptake of radioactivity in all brain regions.

In agreement with the dynamic scans, whole-body PET/CT imaging at 1 and 24 h after infusion (Figs. 4A–4C) revealed uptake to be highest in the BBBO/IA group, reaching 20.44 ± 3.29 %ID/cm^3 and 16.91 ± 1.67 %ID/cm^3 at 1 and 24 h after injection, respectively. Uptake in the IA/BBBI group was 9.25 ± 2.54 %ID/cm^3 and 7.18 ± 2.17 %ID/cm^3 in right hemisphere at 1 and 24 h after injection, respectively. Brain uptake was not facilitated in the IV/BBBO group at 1 or 24 h after injection. Because of the long circulation time of ^{89}Zr-BVDFO, relatively high background (heart and lungs) was observed in all 3 groups. There was also uptake around the neck 24 h after infusion, most likely because the surgery to place the catheter triggered wound healing involving neovascularization.

Ex Vivo Biodistribution

To validate the PET/CT imaging results, ^{89}Zr-BVDFO was further evaluated in an ex vivo biodistribution analysis (Fig. 4E). As expected, in the BBBO/IA group we observed high uptake in the ipsilateral hemisphere, at 15.83 ± 2.46 %ID/g, versus only 2.29 ± 0.82 %ID/g in the contralateral hemisphere. The IA/BBBI group showed uptake of 6.23 ± 2.71 %ID/g and 1.59 ± 1.19 %ID/g in the ipsilateral and contralateral hemispheres, respectively. Uptake in both hemispheres of the IV/BBBO group was below 1 %ID/g. In agreement with earlier studies, high uptake was detected in the blood, lungs, spleen, liver, and thymus (*23*).

DISCUSSION

We observed a linear increase in the concentration of ^{89}Zr-BVDFO in the brain during intraarterial infusion even with an intact BBB, and this concentration was maintained until 24 h after injection. Our finding differs radically from that with iron oxide nanoparticles or small molecules such as salicylic acid derivatives, which immediately clear from the cerebral circulation after intraarterial infusion (*24*). The osmotic BBB opening strongly enhanced uptake of ^{89}Zr-BVDFO only after intraarterial infusion, not after intravenous infusion. Intravenous delivery of ^{89}Zr-BVDFO did not result in any cerebral uptake in naïve mice regardless of BBB status, as agrees with a similar study on mice bearing an orthotopic model of diffuse intrinsic pontine glioma in which no accumulation of ^{89}Zr-BVDFO—either in the brain or in tumors—was observed on intravenous administration (*18*). Intravenous delivery of ^{89}Zr-BVDFO 2 wk after irradiation revealed some uptake in 5 of 7 patients with diffuse intrinsic pontine glioma, but it was characterized by high heterogeneity and only loosely correlated with MR-enhanced territories (*25*). Interestingly, there was no specific signal in the brain 1 h after infusion, but a subsequent increase in signal was observed over the next 144 h. The observed uptake of ^{89}Zr-BVDFO might

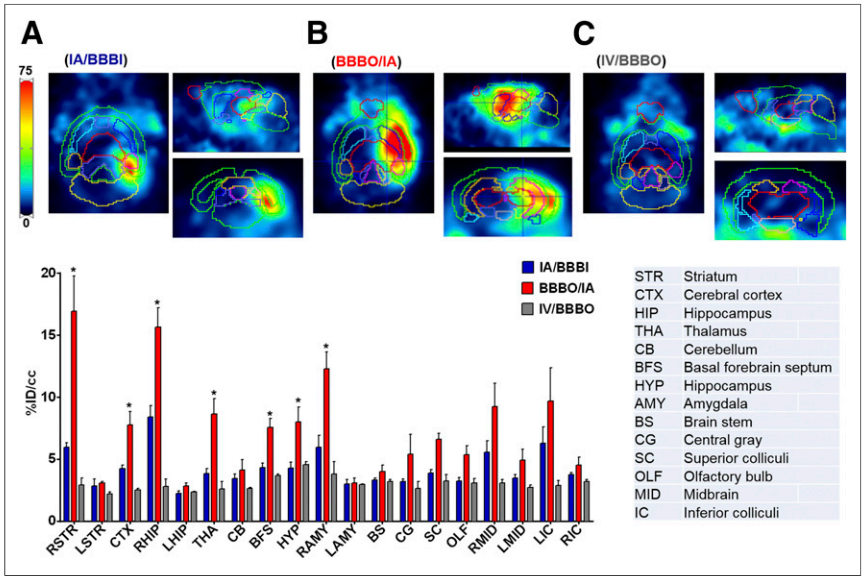

FIGURE 3. Distribution of ^{89}Zr-BVDFO in brain. Representative coronal, sagittal, and transverse PET images overlaid by mouse brain template are shown for IA/BBBI (A), BBBO/IA (B), and IV/BBBO (C). Uptake of ^{89}Zr-BVDFO is significantly higher with BBBO/IA than with IA/BBBI or IV/BBBO and is highest in right striatum, hippocampus, and amygdala. *Statistically significant difference.

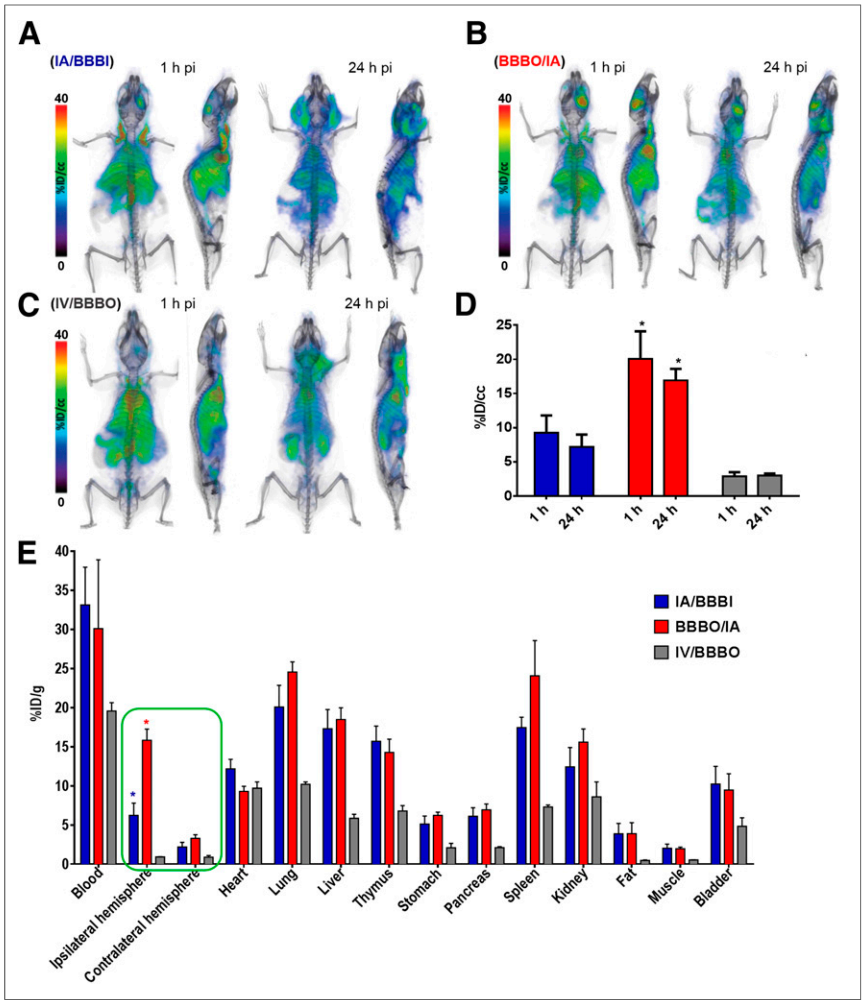

FIGURE 4. ^{89}Zr-BVDFO delivery to, and its biodistribution in, brain with and without BBB opening. (A–C) Representative whole-body PET/CT images obtained with IA/BBBI (A), BBBO/IA (B), and IV/BBBO (C). (D) PET-based quantification of ^{89}Zr-BVDFO uptake in ipsilateral hemisphere. (E) Ex vivo biodistribution 24 h after infusion, showing agreement with higher uptake in ipsilateral than contralateral hemisphere in BBBO/IA group and with higher brain uptake in BBBO/IA group than in IA/BBBI and IV/BBBO groups.

be related rather to radiation-induced vascular injury and subsequent VEGF expression than to tumor-specific accumulation.

The superiority of intraarterial delivery observed in our study aligns well with the rapid growth of applications for endovascular neurointerventions, such as thrombectomy for ischemic stroke (*26*). A recently described method for highly predictable and spatially precise targeting of stem cells (*27*) and the territory of BBB opening (*28*) using real-time MRI guidance promotes wider application of endovascular neurointerventions beyond vascular diseases.

Currently, because of the growing interest in immunotherapies, monoclonal antibodies are widely applied as potent tools in many neoplastic disorders. The simplicity of antibody radiolabeling provides an opportunity to gain insight into their biodistribution at the level of the individual patient. Imaging of biodistribution is particularly compelling when difficult targets such as brain tumors are concerned. Although PET requires radiolabeling, there are reports of a new label-free approach based on chemical exchange saturation transfer MRI (*29*). However, this approach, in which certain drugs produce an internal contrast suitable for detection after intraarterial infusion, has a relatively low sensitivity, and nuclear medicine techniques currently remain the only reliable option for detecting antibodies.

Although our study provides a compelling case in favor of the intraarterial route for delivery of bevacizumab, the study is not devoid of limitations. We studied only one antibody; a different biodistribution might be shown by other antibodies—and likely by other molecules such as single-domain antibodies or dendrimers. We also limited the observation time to 24 h, but in view of the long half-life of antibodies (≤1–2 mo), a significantly longer follow-up period would be worthwhile. In addition, we used naïve animals to test our hypothesis, and we reported only on biodistribution; an ultimate goal would be to use our method to prove that intraarterial delivery has a superior therapeutic effect, especially in correlation with brain uptake of therapeutic agents as measured by PET. Another limitation is that we used only one concentration of antibody and did not study the dependence of brain uptake on antibody concentration. Finally, although it is logical to start from small animals, our positive results might be not true for large animals or, ultimately, for patients; caution must therefore be used in interpreting these results until more advanced studies are performed.

CONCLUSION

Our results indicate that BBBO/IA is a viable route by which to deliver therapeutically relevant amounts of large entities such as antibodies to the brain. Combined with PET—and ultimately PET/MR for precise, real-time assessment of the delivery site of interest—BBBO/IA may present a safe and effective method of managing, and applying endoradiotherapy for, patients with central nervous system malignancies such as GBM.

DISCLOSURE

This work was funded by NIH R01NS091100, NIH R01NS091110, R21NS106436, MSCRFD-3942, and NIH EB024495. No other potential conflict of interest relevant to this article was reported.

REFERENCES

1. Shergalis A, Bankhead A III, Luesakul U, Muangsin N, Neamati N. Current challenges and opportunities in treating glioblastoma. *Pharmacol Rev.* 2018;70:412–445.
2. Jahangiri A, Chin AT, Flanigan PM, Chen R, Bankiewicz K, Aghi MK. Convection-enhanced delivery in glioblastoma: a review of preclinical and clinical studies. *J Neurosurg.* 2017;126:191–200.
3. Grossman R, Burger P, Soudry E, et al. MGMT inactivation and clinical response in newly diagnosed GBM patients treated with Gliadel. *J Clin Neurosci.* 2015;22:1938–1942.

4. Morshed RA, Cheng Y, Auffinger B, Wegscheid ML, Lesniak MS. The potential of polymeric micelles in the context of glioblastoma therapy. *Front Pharmacol.* 2013;4:157.
5. Hersh DS, Kim AJ, Winkles JA, Eisenberg HM, Woodworth GF, Frenkel V. Emerging applications of therapeutic ultrasound in neuro-oncology: moving beyond tumor ablation. *Neurosurgery.* 2016;79:643–654.
6. Burkhardt JK, Riina HA, Shin BJ, Moliterno JA, Hofstetter CP, Boockvar JA. Intra-arterial chemotherapy for malignant gliomas: a critical analysis. *Interv Neuroradiol.* 2011;17:286–295.
7. Owens G. Arterial perfusion of the isolated canine brain. *Am J Physiol.* 1959;197: 475–477.
8. Hatiboglu I, Owens G. Results of intermittent, prolonged infusion of nitrogen mustard into the carotid artery in twelve patients with cerebral gliomas. *Surg Forum.* 1961;12:396–398.
9. Neuwelt EA, Frenkel EP, Diehl JT, et al. Osmotic blood-brain barrier disruption: a new means of increasing chemotherapeutic agent delivery. *Trans Am Neurol Assoc.* 1979;104:256–260.
10. Shapiro WR, Green SB, Burger PC, et al. A randomized comparison of intra-arterial versus intravenous BCNU, with or without intravenous 5-fluorouracil, for newly diagnosed patients with malignant glioma. *J Neurosurg.* 1992;76:772–781.
11. Riina HA, Fraser JF, Fralin S, Knopman J, Scheff RJ, Boockvar JA. Superselective intraarterial cerebral infusion of bevacizumab: a revival of interventional neuro-oncology for malignant glioma. *J Exp Ther Oncol.* 2009;8:145–150.
12. Joshi S, Ellis JA, Ornstein E, Bruce JN. Intraarterial drug delivery for glioblastoma multiforme: will the phoenix rise again? *J Neurooncol.* 2015;124:333–343.
13. Burkhardt JK, Santillan A, Hofstetter CP, et al. Intra-arterial bevacizumab with blood brain barrier disruption in a glioblastoma xenograft model. *J Exp Ther Oncol.* 2012;10:31–37.
14. Chakraborty S, Filippi CG, Burkhardt JK, et al. Durability of single dose intra-arterial bevacizumab after blood/brain barrier disruption for recurrent glioblastoma. *J Exp Ther Oncol.* 2016;11:261–267.
15. Mammatas LH, Verheul HM, Hendrikse NH, Yaqub M, Lammertsma AA, Menke-van der Houven van Oordt CW. Molecular imaging of targeted therapies with positron emission tomography: the visualization of personalized cancer care. *Cell Oncol (Dordr).* 2015;38:49–64.
16. Vosjan MJ, Perk LR, Visser GW, et al. Conjugation and radiolabeling of monoclonal antibodies with zirconium-89 for PET imaging using the bifunctional chelate p-isothiocyanatobenzyl-desferrioxamine. *Nat Protoc.* 2010;5:739–743.
17. Gaykema SB, Brouwers AH, Lub-de Hooge MN, et al. ^{89}Zr-bevacizumab PET imaging in primary breast cancer. *J Nucl Med.* 2013;54:1014–1018.
18. van Es SC, Brouwers AH, Mahesh SVK, et al. ^{89}Zr-bevacizumab PET: potential early indicator of everolimus efficacy in patients with metastatic renal cell carcinoma. *J Nucl Med.* 2017;58:905–910.
19. Bahce I, Huisman MC, Verwer EE, et al. Pilot study of Zr-89-bevacizumab positron emission tomography in patients with advanced non-small cell lung cancer. *EJNMMI Res.* 2014;4:35.
20. Jansen MH, Veldhuijzen van Zanten SEM, van Vuurden DG, et al. Molecular drug imaging: ^{89}Zr-bevacizumab PET in children with diffuse intrinsic pontine glioma. *J Nucl Med.* 2017;58:711–716.
21. Jansen MH, Lagerweij T, Sewing AC, et al. Bevacizumab targeting diffuse intrinsic pontine glioma: results of ^{89}Zr-bevacizumab PET imaging in brain tumor models. *Mol Cancer Ther.* 2016;15:2166–2174.
22. Jablonska A, Shea DJ, Cao S, et al. Overexpression of VLA-4 in glial-restricted precursors enhances their endothelial docking and induces diapedesis in a mouse stroke model. *J Cereb Blood Flow Metab.* 2018;38:835–846.
23. Nagengast WB, de Vries EG, Hospers GA, et al. In vivo VEGF imaging with radiolabeled bevacizumab in a human ovarian tumor xenograft. *J Nucl Med.* 2007;48:1313–1319.
24. Song X, Walczak P, He X, et al. Salicylic acid analogues as chemical exchange saturation transfer MRI contrast agents for the assessment of brain perfusion territory and blood-brain barrier opening after intra-arterial infusion. *J Cereb Blood Flow Metab.* 2016;36:1186–1194.
25. Jansen MH, Veldhuijzen van Zanten SEM, van Vuurden DG, et al. Molecular drug imaging: ^{89}Zr-bevacizumab PET in children with diffuse intrinsic pontine glioma. *J Nucl Med.* 2017;58:711–716.
26. Jovin TG, Chamorro A, Cobo E, et al. Thrombectomy within 8 hours after symptom onset in ischemic stroke. *N Engl J Med.* 2015;372:2296–2306.
27. Walczak P, Wojtkiewicz J, Nowakowski A, et al. Real-time MRI for precise and predictable intra-arterial stem cell delivery to the central nervous system. *J Cereb Blood Flow Metab.* 2017;37:2346–2358.
28. Janowski M, Walczak P, Pearl MS. Predicting and optimizing the territory of blood-brain barrier opening by superselective intra-arterial cerebral infusion under dynamic susceptibility contrast MRI guidance. *J Cereb Blood Flow Metab.* 2016;36:569–575.
29. Liu H, Jablonska A, Li Y, et al. Label-free CEST MRI detection of citicoline-liposome drug delivery in ischemic stroke. *Theranostics.* 2016;6:1588–1600.